**SUPPLEMENTARY MATERIALS**

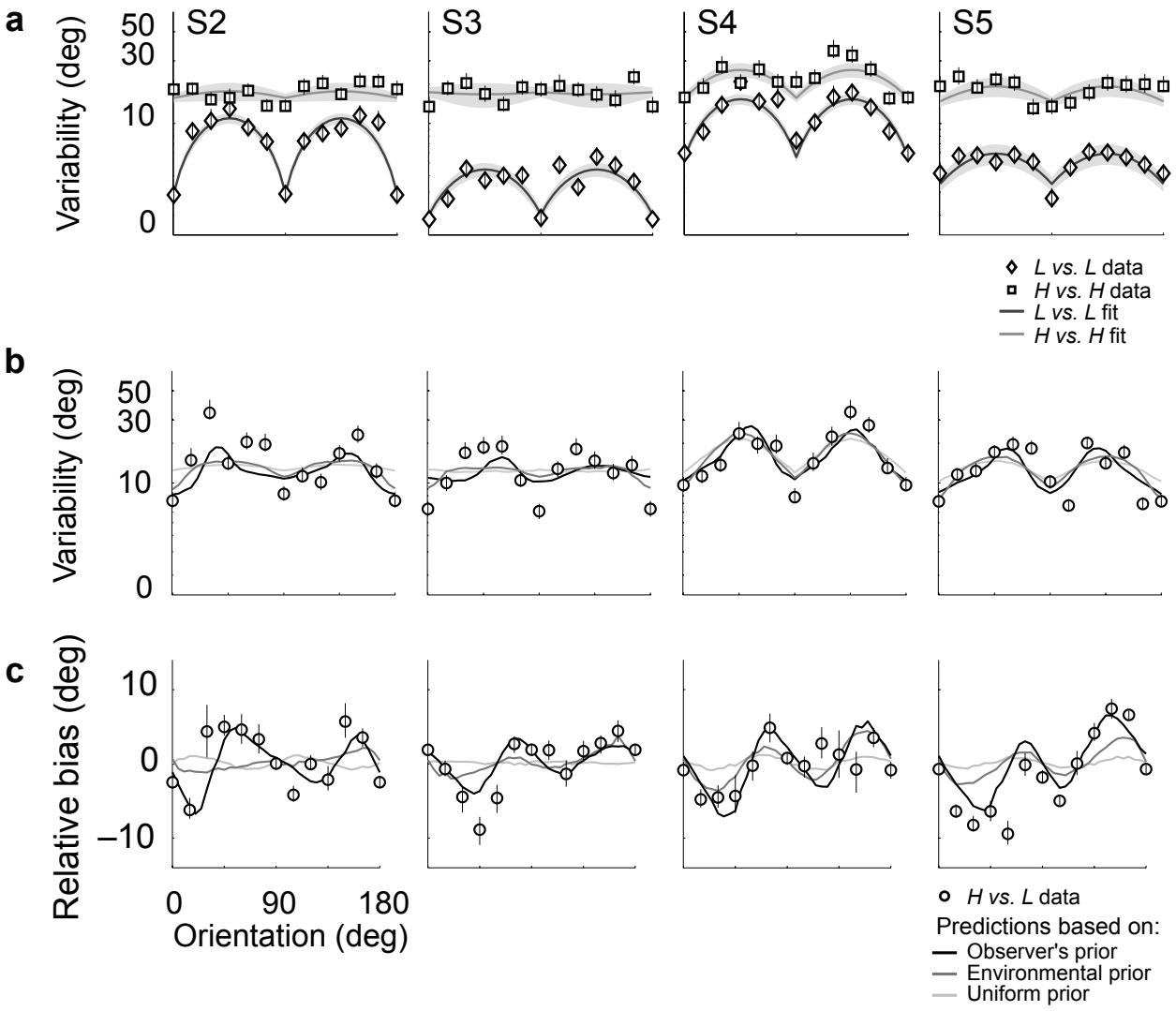


**Supplementary Figure 1** Experimental data for observers S2, S3, S4, and S5 (four columns, respectively). The horizontal axis is orientation (in deg) in all cases. **(a)** Variability of same-noise conditions (*L vs. L* and *H vs. H*). Same format as **Fig. 2b**. (**b**) Cross-noise variability with predictions of three Bayesian-observer models: observers' priors (black), environmental distribution prior (medium gray), and uniform prior (light gray). Same format as **Fig. 5b**. (**c**) Relative bias with the predictions the same three Bayesian-observer models. Same format as **Fig. 5c**.

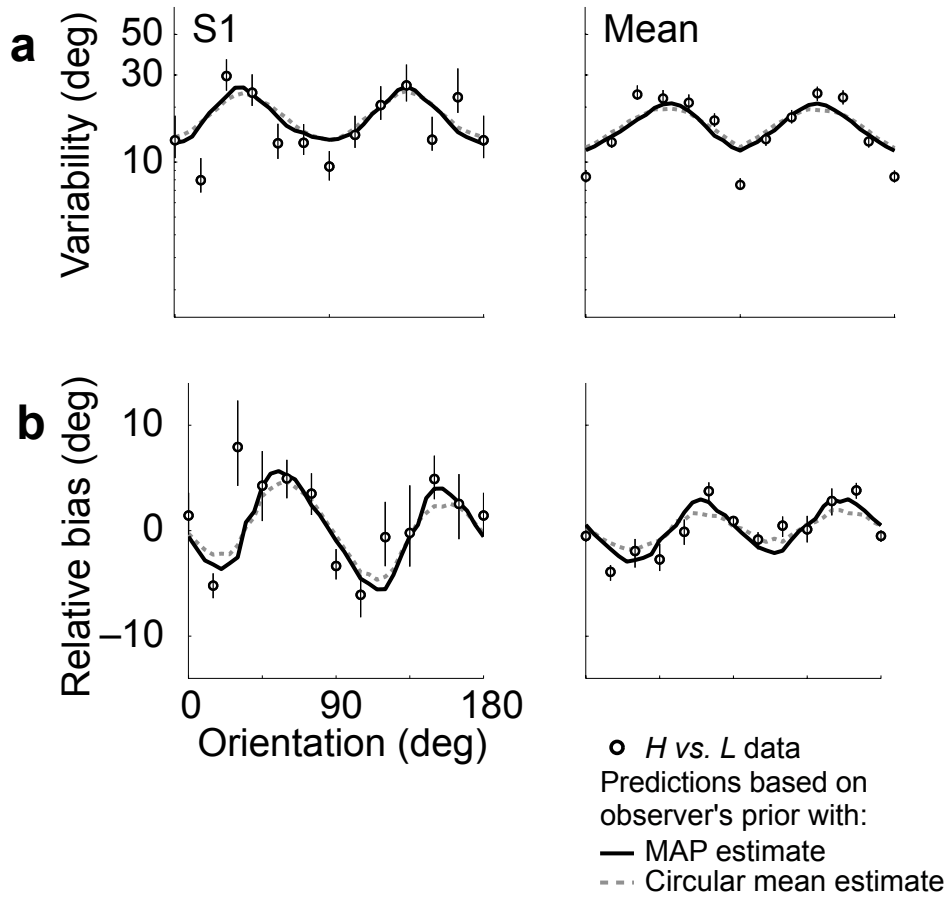


**Supplementary Figure 2** Comparison of two decision rules: *maximum a posteriori* (MAP) and circular mean for representative observer S1 and the mean observer. (**a**) Variability in same format as **Fig. 5b** and **Supplementary Fig. 1b**. (**b**) Relative bias in same format as **Fig. 5c** and **Supplementary Fig. 1c**. Black solid curves (from Fig. 5) are the predictions of the Bayesian observer using the recovered observers' priors and MAP estimation. Gray dashed curves are the predictions of the Bayesian observer using the same recovered observers' priors and a circular mean estimate.The MAP and mean estimates would be identical if the posteriors were symmetric. In our case, the posteriors were asymmetric due to slight asymmetry in the recovered priors and likelihoods.

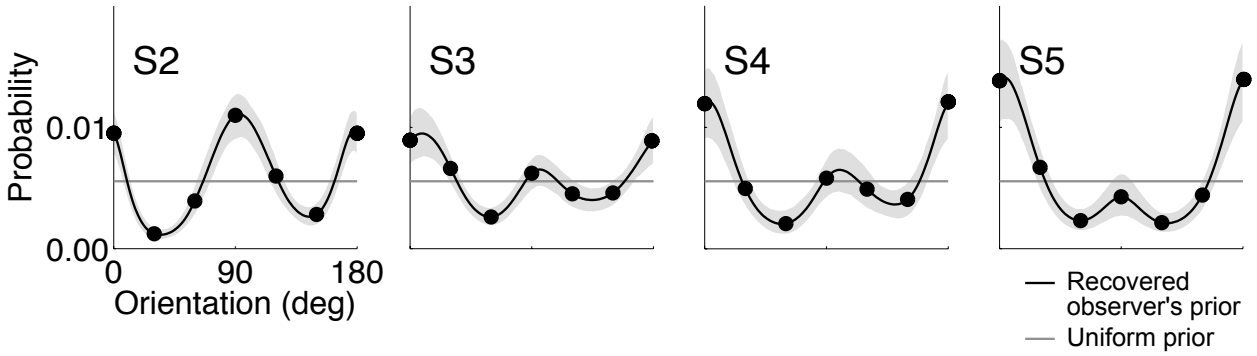


**Supplementary Figure 3** Recovered priors for observers S2, S3, S4, and S5. Same format as Fig. 3.

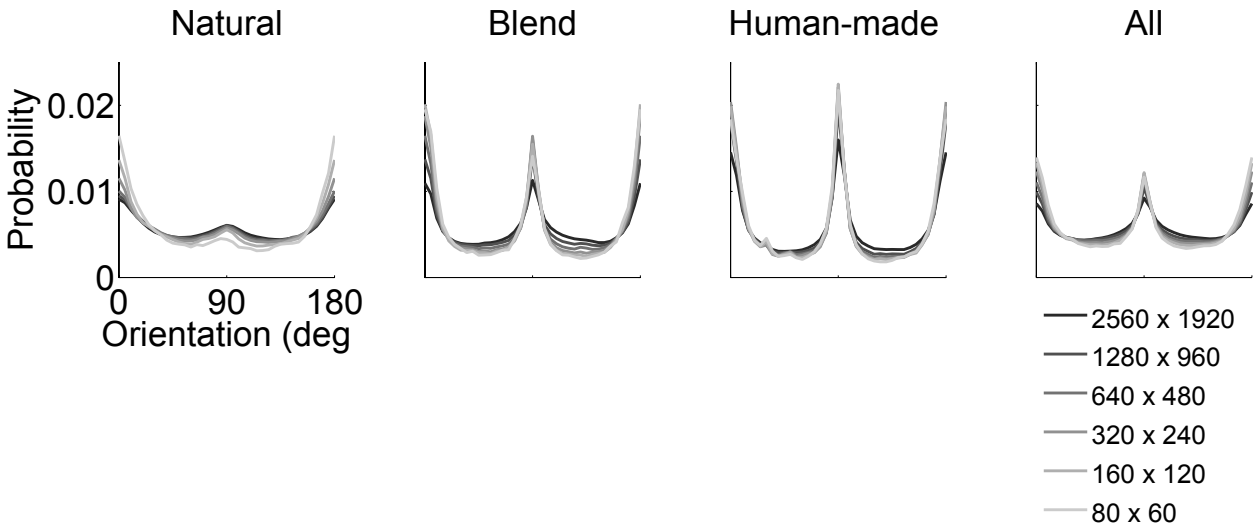


**Supplementary Figure 4** Orientation distributions measured at different scales in a multi-scale decomposition, for four different photographic image collections. From left to right, distributions for photographs containing: mostly natural content (653 images), a blend of natural and human-made content (e.g., a scene with a tree and a house; 151 images), mostly human-made content (221 images), and the full database (1025 images). Human-made scenes are dominated by buildings, and exhibit the sharpest and largest peaks at verticals. Natural scenes, which contain objects such as flowers and foliage, have a reduced dominance of the cardinals and softer peaks. Scenes of blended content lie in-between. Intensity of grey curves corresponds to six image resolutions. The error regions, $\pm$ 1 s.d. from bootstrapping the data 1000 times, are smaller than the line widths.

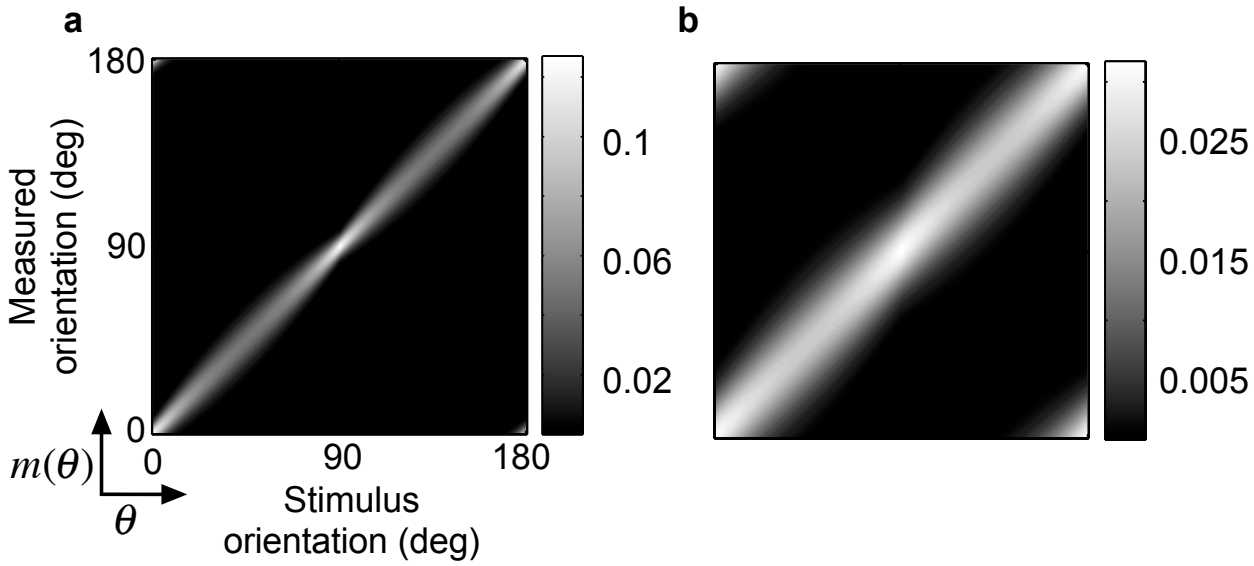


**Supplementary Figure 5** Matrices for the mean observer, in the same format as **Fig. 7**, upper-right panel. Columns are measurement distributions, rows are likelihood functions, and color corresponds to probability. Variance of measurement distributions comes from the fits to the same-noise variability (**Fig. 2b**). Each observer had a corresponding pair of matrices generated from their data. (**a**) Matrix for the low-noise stimuli. Likelihoods are asymmetric, skewed away from the cardinals due to the orientation-dependent change of variance (i.e., the oblique effect). (**b**) Matrix for the high-noise stimuli. Likelihoods are broader and less asymmetric than in **a**. (Note change of scale between **a** and **b.**)